IOP Publishing Journal of Physics D: Applied Physics
J. Phys. D: Appl. Phys. **44** (2011) 000000 (8pp) UNCORRECTED PROOF

Room temperature synthesis of nanocrystalline anatase sols and preparation of uniform nanostructured TiO_2 thin films: optical and structural properties

M Hosseingholi, M Pazouki, A Hosseinnia and S H Aboutalebi

Materials and Energy Research Center, Meshkin Dasht, Karaj, IR Iran

E-mail: mpazouki@merc.ac.ir and mpaz6@yahoo.com

Received 4 October 2010, in final form 15 November 2010
Published
Online at stacks.iop.org/JPhysD/44

Abstract
Transparent TiO_2 thin films were deposited on soda-lime glass substrates via the sol–gel method using a nanocrystalline TiO_2 sol solution prepared at room temperature employing the dip-coating method. The effects of pH on crystallinity, particle size and stability of the synthesized TiO_2 sols were investigated, systematically. TiO_2 thin films were thickened by means of a sequential dip-coating process. The TiO_2 films were transparent and exhibited proper adherence. The effects of thickness and annealing temperature on the structural and optical properties of the thin films were evaluated. The prepared powder was crystalline without any thermal treatment. The crystallite size of (anatase) the particles was in the range 4.2–12.1 nm depending on the initial pH value. Although only anatase phase was observed at room temperature and 400 °C, a further increase in annealing temperature up to 700 °C resulted in the formation of the rutile phase. Even at high annealing temperatures, fairly smooth and homogeneous surfaces with no cracks and pores were observed. It was demonstrated that the films were transparent in the visible region with characteristic absorption in the UV region. Band gap of the as-deposited film was estimated to be 3.34 eV and was found to decrease with increasing annealing temperature.

AQ1 (Some figures in this article are in colour only in the electronic version)

1. Introduction

Owing to its exceptional characteristics such as strong oxidative potential, chemical stability, non-toxicity and good resistance, titanium dioxide (TiO_2) has been receiving increasing attention in recent years compared with other semiconducting materials. Recent advances in the development of new applications for TiO_2 as a photoactive material make it possible to use this fascinating material in a broad range of applications such as antifouling [1, 2], deodorizing [3], antibacterial [4] and self-cleaning applications [5, 6]. TiO_2 (in the form of anatase) offers great potential for use in photocatalytic water splitting, dye-sensitized nanocrystalline solar cells and light-induced hydrophilic surfaces. Hydrophilic TiO_2 films exhibit strikingly high potential for practical applications such as mirrors, window glasses, windshields of automobiles and similar applications [7]. However, to ensure the successful incorporation of TiO_2 films into these applications, three factors should be considered: the absence of scattering of visible light (which usually requires the absence of particles larger than about 30 nm), sufficient abrasion resistance to assure that the film is not damaged when cleaned or when impacted by dust particles, and finally an adequate photooxidation rate [1]. AQ2

A variety of physical and chemical approaches have been used for TiO_2 thin film preparation such as sol–gel [8–10], pulsed laser deposition [11, 12], reactive evaporation [13], reactive sputtering [14] chemical vapour deposition [15, 16] and spray pyrolysis [17, 18]. An interesting, common, facile and cost-effective route to obtain TiO_2 is the use of the sol–gel method which not only omits the requirement for high temperatures, toxic chemicals and expensive equipments but also offers several advantages such as high purity and homogeneity of the final product [19]. However, there are some major drawbacks associated with the use of the sol–gel method for the production of TiO_2. The most important disadvantage comes from the fact that the TiO_2 film obtained from the sol–gel method is usually in the form of an amorphous material which consequently initiates the need for subsequent heat treatment of the obtained material at relatively high temperatures. As a result, some limitations are imposed on the choice of substrate. Although there are some papers reporting the synthesis of anatase crystalline phase at room temperature (RT) [20–22], there are some heat-treatment steps involved in all of them. To the best of the authors' knowledge, this is the first report on the synthesis of anatase crystalline phase at RT without any special heat-treatment steps. The crystallinity of the sols was verified employing the dispersive Raman spectroscopy technique in the as-prepared state.

This work addresses the above-mentioned problem by synthesizing nanocrystalline TiO_2 sols at RT by hydrolysing tetraisopropyl orthotitanate in an acidic aqueous solution. TiO_2 thin films were deposited from the resulting sol at RT by employing a dip-coating process on glass slides. The effects of the acidity of aqueous solution, thickness and annealing temperature are systematically investigated.

2. Experimental

2.1. Materials and synthesis

All chemicals used in this study were of analytical grade, supplied by Merck Chemicals, and were used without further purification.

Nanocrystalline anatase TiO_2 sols were prepared as follows. Tetraisopropyl orthotitanate ($Ti(OCH(CH_3)_2)_4$) (5 ml) was mixed with isopropyl alcohol (95 ml). The resulting solution was added dropwise into de-ionized water (900 ml) which was pH adjusted by HNO_3 (65% w/w) addition. After continuous stirring of the reaction mixture for 20 h, a colloidal solution of TiO_2 nanocrystals was formed which was used to prepare thin films and powders. To investigate the phase transformation after heat treatment at high temperatures, dried titania particles at RT were heated in a furnace for 1 h at 400 and 700 °C.

TiO_2 thin films were deposited on standard soda-lime glass microscope slides ($75 \times 25 \times 1$ mm). Before deposition, the substrates were cleaned in diluted H_2SO_4 and absolute ethanol for 15 min using an ultrasonic bath. Then they were thoroughly rinsed with de-ionized water. A home-made dip-coating apparatus was used for the deposition. The substrates were immersed in the coating solution and then withdrawn at a regulated speed of 2 mm s^{-1}. The coating process was repeated several times to obtain samples with different thicknesses. Upon withdrawing from the sol, the substrates were dried in an oven in air at 90 °C for 5 min. To understand the role of heat treatment, the films were annealed at 200 and 400 °C for 1 h.

2.2. Characterization

The crystalline structure and the average crystallite size of TiO_2 powder were determined by an x-ray diffractometer (Siemens D-500, Philips) with the Cu Kα x-ray tube at 1.54 Å, 30 kV and 25 mA with scan steps of 1° min^{-1} over the 2θ range 20°–80°. Dynamic light scattering (DLS) was used to measure the particle size of the different prepared TiO_2 sols (Horiba LB-550). Raman analysis was conducted in the backscattering configuration. A coherent internal 17 mW He–Ne laser was used as the excitation source. The scattering light was analysed employing a LabRAM HR Raman confocal microscope manufactured by HORIBA Scientific; acquisition time was 60 s. Simultaneous thermal analysis (STA1640 STA 164 PL.Eng) was performed to determine the thermal stability of the powders with a heating rate of 10 °C min^{-1} in an air flow. The topography of the surface was evaluated by atomic force microscopy (AFM) (DME-SPM DualScope DS 95-50/200). The morphology of the TiO_2 films was observed using scanning electron microscopy (SEM) (Streoscan 360, Leica Cambridge) with an accelerating voltage of 20 kV. The chemical structure of the dried gel was examined using a Fourier transform infrared spectrophotometer (FTIR, BRUKER VECTOR 33) in the range 400–4000 cm^{-1}. Optical absorbance and transmittance measurements were carried out using a UV–Vis spectrophotometer (Agilent 8453).

3. Results and discussion

3.1. Structural studies

Figure 1 shows the XRD patterns of the TiO_2 particles obtained from the sols synthesized at different pH values (0.7, 1, 1.5, 2 and 2.5).

Figure 1 presents the characteristic diffraction peaks of anatase phase in all the samples. It can be concluded from table 1 that the calculated anatase phase content and anatase crystallite size increased and decreased, respectively, as the pH value of the aqueous solution decreased. From the stability point of view the sol pH value was proved to be a crucial point because of the fact that only in a certain range of pH value (1–2) a homogeneous suspension of fine particles can be formed whereas outside this range white precipitates can be formed immediately after hydrolysis reaction. A higher acid concentration promotes the hydrolysis rate which in turn leads to larger repulsion due to the promotion and higher uptake of protons which is determined by the pH of the surrounding environment. The surface is assumed to be covered with surface hydroxyl species. Therefore, under higher acidic conditions slower formation of aggregates or clusters favours the the subsequent formation of homogeneous suspensions.

It is commonly accepted that high-temperature annealing, at least at 400 °C, is required to obtain TiO_2 powders in the form of anatase. However, in this work, anatase nanocrystalline particles are prepared at RT without a further heat-treatment process. Figure 2 demonstrates the effect of annealing

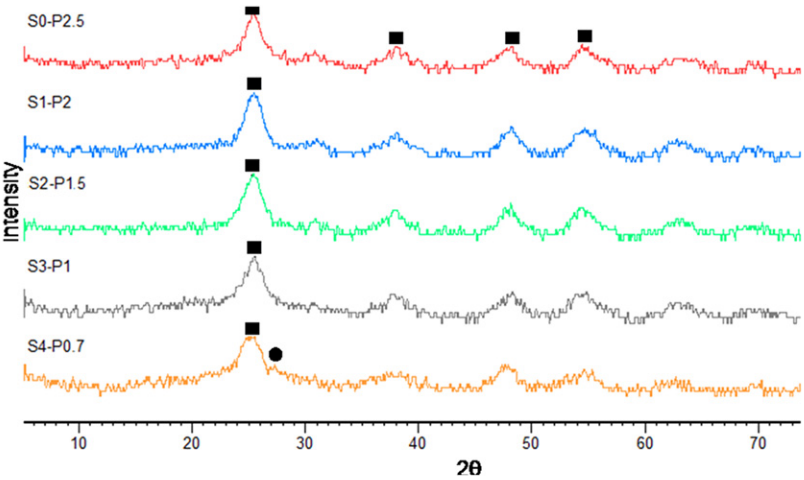

Figure 1. XRD patterns of dried TiO_2 sol samples prepared at different acidities (■: anatase and ●: rutile phase).

Table 1. Synthesis condition, crystallinity and stability of TiO_2 sol and powders obtained at RT.

Name	pH	Appearance	A–B–R%[a]	Anatase crystallite size (nm)	Particle size (nm)	Stability
S0-P2.5	2.5	Light blue transparent sol with small precipitate	73.4–26.6	12.1(±1.9)	24	Precipitate
S1-P2	2	Light blue transparent sol	83–17	7.6(±0.3)	20	More than 1 year
S2-P1.5	1.5	Green transparent sol	85.3–14.7	6.6(±0.3)	—	More than 1 year
S3-P1	1	Green transparent sol	95.5–4.5	4.9(±0.5)	22	More than 1 year
S4-P0.7	0.7	Orange sol with precipitate	91.7–4–4.3	4.2(±0.4)	39	1 week

[a] A—anatase phases; B—brookite phases; R—rutile phases.

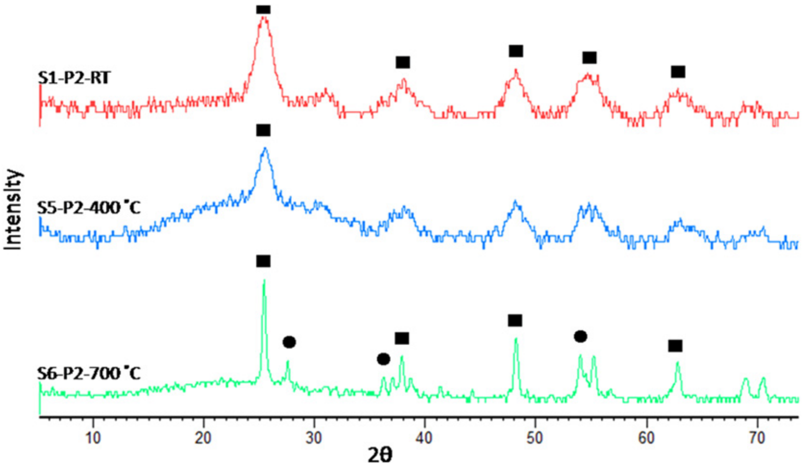

Figure 2. XRD patterns of dried TiO_2 sol samples at pH 2 prepared at different annealing temperatures (■: anatase and ●: rutile phase).

temperature on the crystallite size and the phase of the as-prepared TiO_2 nanoparticles at a constant pH value of 2.

Figure 2 reveals that upon increasing the annealing temperature, not only the size of the formed anatase crystallites has increased but also the formation of rutile phase is promoted resulting in the coexistence of rutile and anatase phases together which can be attributed to the thermally promoted crystallite growth. The size of anatase crystallites increases from 11 nm at 400 °C to 69 nm at 700 °C (table 2). At 700 °C the intensity of anatase peaks is increased, from which it can be inferred that TiO_2 nanoparticles are apparently becoming more crystalline. Therefore, the present results confirm that the powders obtained by air-drying of the as-prepared sol are crystalline in nature, which proves that the formation of the crystalline (anatase) phase readily occurred during the preparation of the solution.

Table 2. Synthesis condition and crystallinity of annealed TiO_2 powders at pH 2.

Name	pH	Temperature (°C)	A–B–R%[a]	Anatase crystallite size (nm)	Rutile crystallite size (nm)
S5-P2	2	400	88–12	10.9(±1.9)	—
S6-P2	2	700	79.5–1.9–18.6	68.9(±4.3)	87.4

[a] A—anatase phases; B—brookite phases; R—rutile phases.

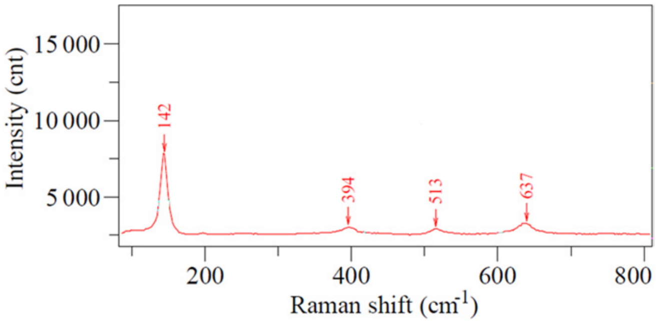

Figure 3. Raman spectra of TiO_2 sol at pH 2.

The crystallite size of the particles was evaluated using the full-width at half-maximum (FWHM) of the most intense diffraction peak of anatase (1 0 1) according to Scherrer's equation:

$$D = \frac{k\lambda}{\beta \cos\theta}, \tag{1}$$

where D is the crystallite size in nm, λ is the wavelength of the x-ray radiation (Cu Kα = 0.154 06 nm), k is a constant taken as 0.94, θ is the Bragg angle taken in radians and β is the (FWHM) line width at half maximum height [23].

Gopal and co-workers [24] reported that the formation of anatase and rutile can be determined by the kinetic behaviour of TiO_2 clusters upon nucleation and growth. If condensation starts before the completion of hydrolysis, either amorphous or metastable anatase TiO_2 is formed. Under neutral and basic conditions, condensation starts before the completion of hydrolysis and the formation of ordered structure is hindered, so the dried gel is amorphous. However, acidic environment promotes the hydrolysis rate which simultaneously results in the decrease in the condensation rate. A higher acid concentration leads to larger repulsion and promotes the slower formation of aggregates or clusters which in turn provides enough reaction time for the formation of the thermodynamically preferred phase of TiO_2, rutile. Therefore, a higher acid concentration promotes the formation of rutile, while a lower acid concentration promotes anatase formation.

Figure 3 shows the Raman spectra of the nanostructured TiO_2 sol prepared at pH 2. The absorption peaks at 637, 513, 394 and 142 cm^{-1} correspond to the characteristic peaks of the anatase phase, suggesting that the anatase TiO_2 sol is obtained at RT. The Raman spectra results are in agreement with XRD measurements.

3.2. Thermal analysis

Figure 4 shows the thermogravimetric analysis (TGA) curve of the sample at pH 2. The weight loss occurred in three temperature regions. The first stage is from RT to 195 °C, over which the mass loss is the highest. A mass loss of up to 11.14% is observed, resulting from the evaporation of water and isopropanol. The second stage is from 195 to 243 °C, where the mass loss is 3.75%; this can be assigned to the combustion and carbonization of most organic contents in the powders. The third stage is from 243 to 360 °C, where the mass loss is 3.61%, which can be attributed to further combustion of the remaining organic compounds and evaporation of chemisorbed water.

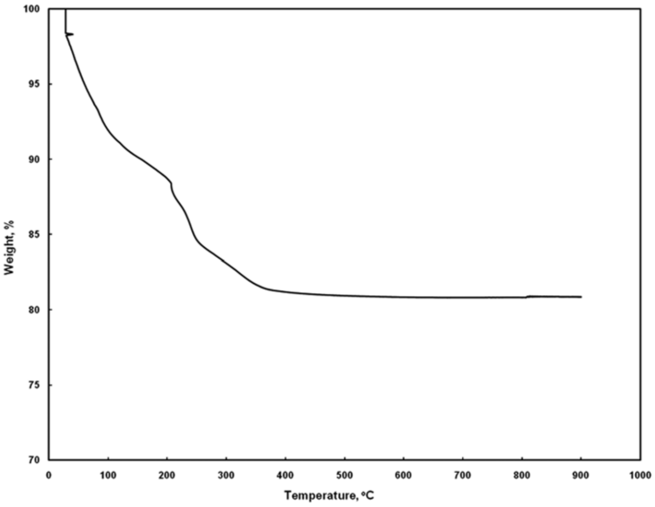

Figure 4. TGA curve of TiO_2 powder at pH 2 from ambient temperature up to 900 °C.

3.3. Robustness

All deposited TiO_2 films at pH 2 were found to exhibit very good adhesion properties based on the Scotch tape test [25] and the pencil hardness test. The deposited films cannot be removed even after boiling in 1M KOH. In comparison, the TiO_2 films deposited at a pH value of around 0.7 can be easily removed from the surface upon scratching with pencil. Moreover, investigation of the stability of films deposited at pH 2 after 1 year demonstrated the same trend which proves that even after long periods of time after deposition, the films were pretty stable.

3.4. Morphological characterization

AQ3

Thickness of the prepared films was evaluated using AFM. Figure 5 shows the cross section of the as-deposited film obtained after 15 cycles of dip-coating deposition. The average thickness of the films is shown in table 3. The thickness increased fairly linearly with the number of cycles

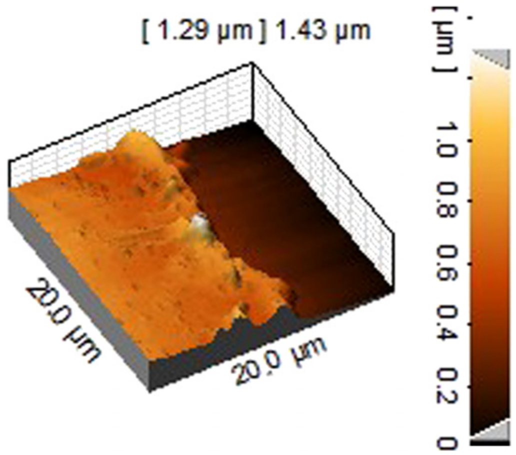

Figure 5. Cross-section image of TiO_2 film coated for 25 times.

Table 3. Thickness, roughness and average grain size of deposited TiO_2 films at pH 2 at different temperatures.

Name	Thickness (nm)	Roughness (nm)	Average grain size (nm)
5 times coated-RT	65	4.55 (±0.14)	52.60 (±1.73)
15 times coated-RT	188	9.87 (±2.75)	72.76 (±6.68)
15 times coated-200 °C	—	21.3 (±1.70)	235.08 (±2.24)
15 times coated-400 °C	—	27.4 (±5.66)	282.50 (±13.43)
25 times coated-RT	331	13.5 (±2.62)	88.02 (±8.61)

of dip-coating. The average film thickness per coating cycle is estimated to be about 13 nm.

Figures 6(*a*)–(*c*) illustrate the three-dimensional (3D) AFM images of the TiO_2 thin films deposited on glass substrates at pH 2 before annealing, and dip-coated for 5, 15 and 25 cycles, respectively. All the films are quite rough on the nanometre scale, with a granular structure consisting of interconnected grain particles fused together.

Multiple scans of several dimensions were collected at different locations on the surface in order to ensure that the result obtained is representative of the whole surface. However, all roughness measurements were made on $5 \times 5\,\mu$m scans for each sample, allowing direct comparison of measurements on different samples. The surface roughness in the films increases with thickness which is shown in table 3 due to the increase in the grain size. The 25-time coated film exhibited much rougher surface, which is readily favourable for the adsorption of organic pollutants.

AFM images of the as-deposited and annealed 15-cycle deposited TiO_2 films at different temperatures are shown in figure 7. The surfaces of the annealed films are composed of uniform and spherical grain structures in contrast with the surface of the as-deposited film which exhibits concave–convex structures of nanoparticles. The AFM analysis of the TiO_2 films showed that the surface roughness of the films increased after annealing due to the increase in grain size of particles as shown in table 3.

Figure 8 shows the SEM images of the surface of the TiO_2 films prepared by 1 and 5 coating cycles at pH 2 without heat treatment and heat treated at 400 °C for 1 h. The films coated at different coating cycles exhibited granular structure with distinct grain boundaries and flat texture. Although increasing the coating cycle results in an increase in thickness, it showed no visible effect on the uniformity of the films. However, the grains fused into each other with increasing temperature. The SEM micrographs indicated a well-adhered, dense and crack-free TiO_2 films on glass over a wide area even at high temperatures. These films exhibited morphological homogeneity.

3.5. FT-IR spectra

Figure 9 shows the FT-IR spectrum of the dried sol at pH 0.7 annealed at different temperatures in the range 400–4000 cm^{-1}.

FTIR analysis clearly demonstrates the existence of Ti–O band (peaks in the region 400–800 cm^{-1}) [26] and its promotion upon increase in temperature. In contrast with the sample at pH 2 in which the rutile phase appears at heat-treatment temperatures above 700 °C, the rutile phase here appears at a lower heat-treatment temperature, 400 °C (426 cm^{-1}) [27]. The sharp peak at 1380 cm^{-1} is due to the presence of nitrates, which were added as HNO_3 during the acidification in the sol–gel synthesis. This peak disappeared at high temperatures. In addition, the broad absorption peak at 3411 cm^{-1} is related to a stretching vibration of hydroxyl groups on different sites and to varying interactions between hydroxyl groups on the TiO_2 surface, while the peak at 1640 cm^{-1} is assigned to the bending vibrations of adsorbed H_2O molecules. The significant decrease in OH band intensities at high temperatures is an indication of the fact that the physisorbed water is easily removed from the surface, but the decrease in the OH band intensities bonded to TiO_2 may be attributed to the OH population produced by a dehydroxylation of the surface titania [28]. However, this peak is observed in the FT-IR profiles of all the samples, which is due to the existence of residual OH groups bonded with Ti in the samples [19].

3.6. Optical characterization

Figure 10 shows the UV–Vis transmittance spectra of the films deposited on glass after 1, 5, 10, 15 and 25 dip-coating cycles, respectively. Upon increasing the number of deposition cycles, and consequently the thickness of the layers, absorption is enhanced which subsequently results in a red shift in the absorption edge of the films and a decrease in the transmittance of the TiO_2 films. The absorption edge of the films shifted towards longer wavelengths with increasing thickness. The shift can be ascribed to the difference in crystallite size. The thinnest films which underwent a shorter thermal treatment contained relatively small crystallites and were blue shifted.

The transmittance of the TiO_2 thin film is slightly less than that of the uncoated substrate. Relatively high transmittance of the films up to 10 coating cycles indicates their low surface roughness and good homogeneity which is in contrast with the coatings produced with above 10 cycles.

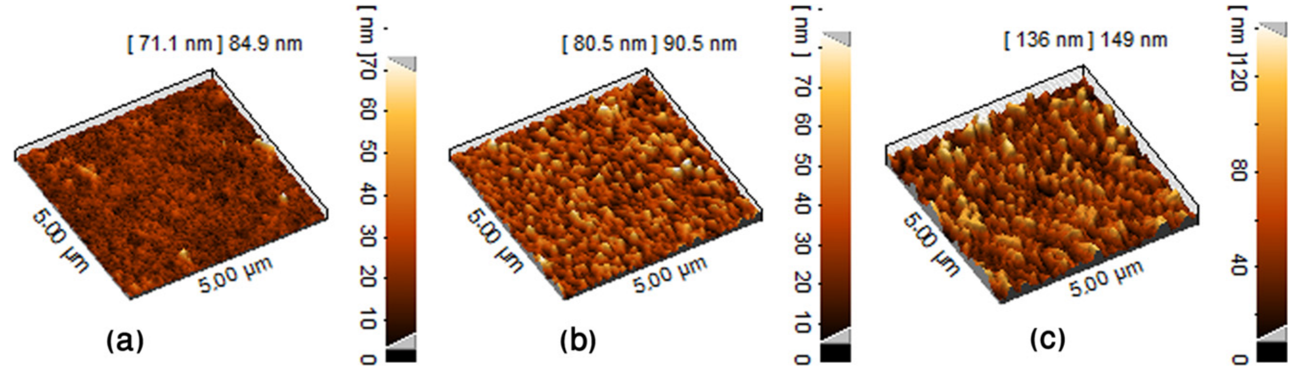

Figure 6. AFM images of as-deposited TiO_2 film on glass substrates at different thicknesses: (*a*) 5-cycle, (*b*) 15-cycle and (*c*) 25-cycle deposited.

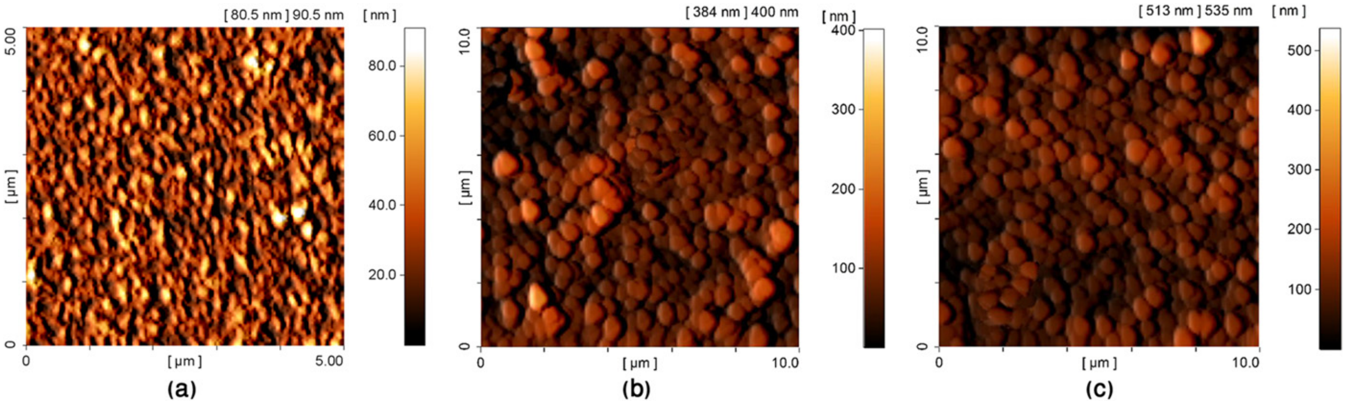

Figure 7. AFM images of 15-cycle deposited TiO_2 film on glass substrates annealed at different temperatures: (*a*) as deposited, and annealed at (*b*) 200 °C and (*c*) 400 °C.

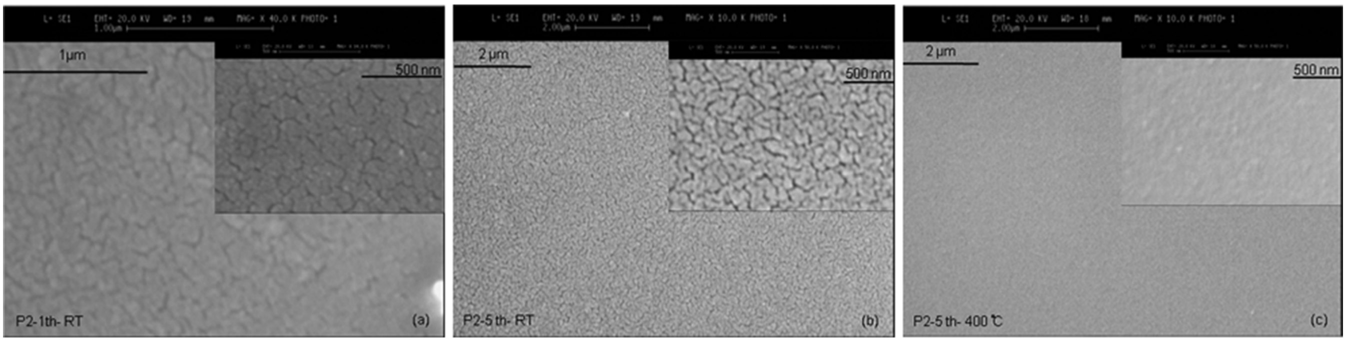

Figure 8. SEM images of 1-cycle at (*a*) RT and 5-cycle dip-coated film at (*b*) RT and (*c*) 400 °C for deposited film at pH 2

The UV–Vis spectra were processed in order to obtain the energy band gap E_g. The band gap E_g was calculated using the Tauc equation:

$$\alpha = \frac{k(h\upsilon - E_g)^n}{h\upsilon}, \qquad (2)$$

where α is the absorption coefficient (cm^{-1}) and $h\upsilon$ is the photon energy (eV), k is a constant, and the value of n can be 0.5 or 2 depending on whether it is a direct or indirect transition. The optical band gap was estimated by extrapolating the straight line portion of the $(\alpha h\upsilon)^{1/2}$ versus $h\upsilon$ plot (figure 11). The band gap calculated based on the absorption spectra demonstrates (table 4) that the band gap of the as-deposited sample for 5 cycles was 3.34 eV, while after annealing at 200 °C and 400 °C it decreased to 3.28 eV and 3.22 eV, respectively.

Also the blue shift in the band gap could be observed in the films produced after 1, 4 and 5 cycles which can be associated with the nanocrystalline nature of the films. However, for the films produced after at least 10 dip-coating cycles, band gap values correspond to bulk anatase.

Table 5 shows the transmittance obtained for the as-deposited and annealed films produced at different cycles upon annealing at 200 and 400 °C. It is evident from table 5 that the as-deposited and annealed films with a small thickness are highly transparent (transmittance is above 88%) in the visible region. However increasing the annealing temperature

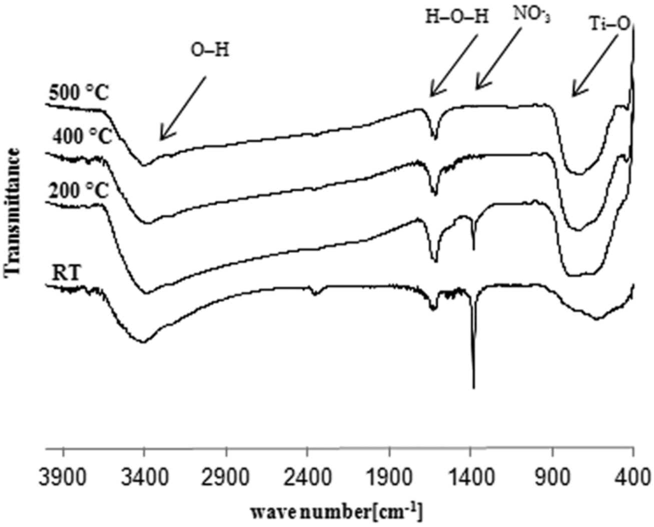

Figure 9. FT-IR spectra of nanosized TiO_2 powders obtained of pH 0.7 sol annealed at different temperatures.

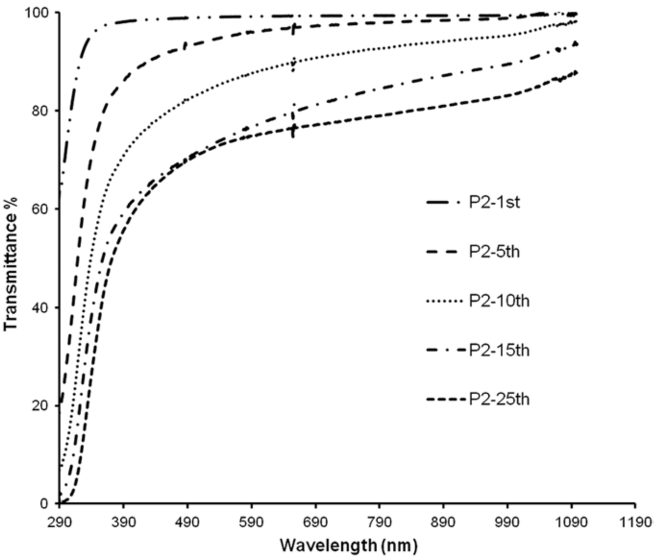

Figure 10. UV–Vis transmission spectra of TiO_2 thin films prepared at pH 2 with different number of coating cycles (1, 5, 10, 15, 25).

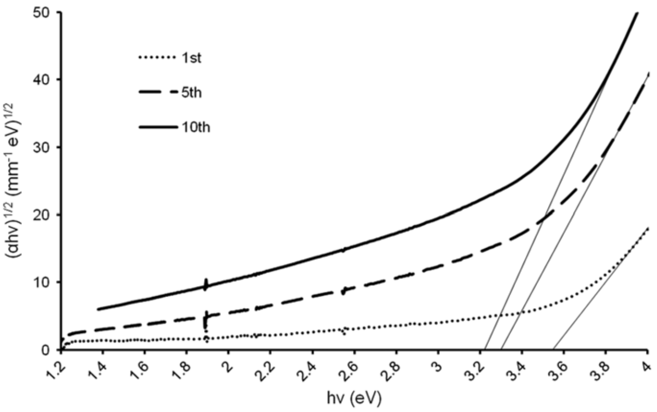

Figure 11. Plot of optical variation of $\alpha^{1/2}$ versus $h\nu$ of TiO_2 thin film with different coating cycles (1, 5 and 10).

Table 4. Band gap of TiO_2 thin films prepared under different conditions.

Sample names	Band gap energy (eV)-RT	Band gap energy (eV)-200 °C	Band gap energy (eV)-400 °C
1st	3.55	3.51	3.49
4th	3.53	3.47	3.38
5th	3.34	3.28	3.22
10th	3.22	3.16	3.04

Table 5. Transmittance of TiO_2 thin films prepared under different conditions.

Sample names	%Transmittance at 410 nm-RT	%Transmittance at 410 nm-200 °C	%Transmittance at 410 nm-400 °C
1st	98.45	98.32	97.78
4th	91.54	91.10	90.62
5th	88.63	88.29	89.50
10th	81.08	74.31	75.56
15th	62.51	68.12	55.62
20th	61.91	57.38	55.51
25th	60.15	55.91	51.71

not only results in a decrease in the transmission value but also causes red shift in the absorption edge which directly results in a decrease in the band gap value. The decrease in the optical band gap of the TiO_2 films upon increasing the annealing temperature might be the direct result of the change in film density and increase in grain size typically associated with annealing at higher temperatures.

4. Conclusion

Nanocrystalline TiO_2 sols were synthesized by hydrolysis of tetraisopropyl orthotitanate at different pH values at room temperature. Robust and transparent nanocrystalline TiO_2 thin films were deposited on glass slides by a dip-coating method from the anatase TiO_2 sols. The obtained films were of good quality, and exhibited smooth and crack-free surfaces even at high temperatures. Also, the thin films showed high transmittance at low thickness values. In summary, anatase TiO_2 sols obtained by the sol–gel method presented here can be easily introduced to temperature-sensitive substrates, which are prone to heat-treatment processes usually required to form anatase sols, and will open a new door of possibilities to introduce anatase into temperature-sensitive substrates. Furthermore, annealing is usually accompanied with thermally induced grain growth and fusion of particles into each other which subsequently results in further grain growth and consequently limited control on particle size; however, processing anatase sols at room temperature gives us the degree of control required for the efficient processing of anatase particles.

Acknowledgments

The authors acknowledge the support from Horiba Scientific and Mahar Fan Abzar Co. for performing the Raman Analysis and AFM measurements, respectively. The authors also thank

Dr A Zolfaghari Hesari from the Chemistry and Chemical Research Institute of Iran for his support with UV–Vis instrumentation and fruitful discussions.

AQ4

References

[1] Paz Y, Luo Z, Rabenberg L and Heller A 1995 *J. Mater. Res.* **10** 2842–48

[2] Mills A and Wang J 2006 *J. Photochem. Photobiol.* A **182** 181–6

[3] Sopyan I, Watanabe M, Murasawa S, Hashimoto K and Fujishima A 1996 *J. Electroanal. Chem.* **415** 183–6

[4] Evans P and Sheel D W 2007 *Surf. Coat. Technol.* **201** 9319–24

[5] Euvananont C, Junin C, Inpor K, Limthongkul P and Thanachayanont C 2008 *Ceram. Int.* **34** 1067–71

[6] Bozzi A, Yuranova T, Guasaquillo I, Laub D and Kiwi J 2005 *J. Photochem. Photobiol.* A **174** 156–64

[7] Özenbaş M and Kaya Ö 2004 *Key Eng. Mater.* **264–268** 505–8

[8] Brinker C J and Harrington M S 1981 *Sol. Energy Mater.* **5** 159–72

[9] Fan Q, McQuillin B, Ray A K, Turner M L and Seddon A B 2000 *J. Phys. D: Appl. Phys* **33** 2683–86

[10] Garzella C, Comini E, Tempesti E, Frigeri C and Sberveglieri G 2000 *Sensors Actuators* B **68** 189–96

[11] Yamamoto S, Sumita T, Sugiharuto, Miyashita A and Naramoto H 2001 *Thin Solid Films* **401** 88–93

[12] Suda Y, Kawasaki H, Ueda T and Ohshima T 2005 *Thin Solid Films* **475** 337–41

[13] Mergel D, Buschendorf D, Eggert S, Grammes R and Samset B 2000 *Thin Solid Films* **371** 218–24

[14] Viseu T M R and Ferreira M I C 1999 *Vacuum* **52** 115–20

[15] Nolan M G, Pemble M E, Sheel D W and Yates H M 2006 *Thin Solid Films* **515** 1956–62

[16] Yeung K S and Lam Y W 1983 *Thin Solid Films* **109** 169–78

[17] Kavitha R, Meghani S and Jayaram V 2007 *Mater. Sci. Eng.* B **139** 134–40

[18] Oja I, Mere A, Krunks M, Nisumaa R, Solterbeck C H and Es-Souni M 2006 *Thin Solid Films* **515** 674–77

[19] Sun L, An T, Wan S, Li G, Bao N, Hu X, Fu J and Sheng G 2009 *Sep. Purif. Technol.* **68** 83–9

[20] Wang P, Xie T, Peng L, Li H, Wu T, Pang S and Wang D 2008 *J. Phys. Chem.* C **112** 6648–52

[21] Ren D, Cui X, Shen J, Zhang Q, Yang X, Zhang Z and Ming L 2004 *J. Sol–Gel Sci. Technol.* **29** 131–6

[22] Zhou Y and Antonietti M 2003 *J. Am. Chem. Soc.* **125** 14960–1

[23] Cullity B D 1978 *Elements of X-ray Diffraction* (London: Addison-Wesley)

[24] Gopal M, Moberly Chan W J and Jonghe L C D 1997 *J. Mater. Sci.* **32** 6001–8

[25] Manning T D, Parkin I P, Clark R J H, Sheel D W, Pemble M E and Vernardou D 2002 *J. Mater. Chem.* **12** 2936–9

[26] Liu H, Cheng X, Yang J, Yan X and Shi H 2007 *J. Mater. Sci. Technol.* **23** 123–6

[27] Djaoued Y, Badilescu S, Ashrit P V, Bersani D, Lottici P P and Bruning R 2002 *J. Sol–Gel Sci. Technol.* **24** 247–54

[28] Pecchi G, Reyes P, Sanhueza P and Villaseñor J 2001 *Chemosphere* **43** 141–6

QUERIES

Page 1
AQ1
Please be aware that the colour figures in this article will only appear in colour in the web version. If you require colour in the printed journal and have not previously arranged it, please contact the Production Editor now.

Page 1
AQ2
Please confirm whether ‘dust’ as set is correct instead of ‘duct’ in ‘However, to ensure the successful incorporation...’.

Page 4
AQ3
The caption of figure 5 says ‘25 times’ and not ‘15’; please clarify.

Page 8
AQ4
Please check the details for any journal references that do not have a blue link as they may contain some incorrect information. Pale purple links are used for references to arXiv e-prints.